Stochastic Synchrony of Chaos in a Pulse Coupled Neural Network with Both Chemical and Electrical Synapses among Inhibitory Neurons

Takashi Kanamaru† and Kazuyuki Aihara‡,††

† Department of Innovative Mechanical Engineering,
Faculty of Global Engineering, Kogakuin University,
139 Inume, Hachioji-city, Tokyo 193-0802, Japan

‡ Institute of Industrial Science, University of Tokyo,
4-6-1 Komaba, Meguro-ku, Tokyo 153-8505, Japan

†† ERATO, JST, Japan

Neural Computation, vol.20, no.8 (2008) pp.1951-1972.
Java Applet: http://brain.cc.kogakuin.ac.jp/~kanamaru/Chaos/e/sSync/

Abstract

The synchronous firing of neurons in a pulse coupled neural network composed of excitatory and inhibitory neurons is analyzed. The neurons are connected by both chemical synapses and electrical synapses among the inhibitory neurons. By introducing electrical synapses, periodically synchronized firing as well as chaotically synchronized firing is widely observed. Moreover, we find stochastic synchrony where the ensemble-averaged dynamics shows synchronization in the network but each neuron has a low firing rate and the firing of the neurons seems to be stochastic. Stochastic synchrony of chaos corresponding to a chaotic attractor is also found.

1 Introduction

Since the 1980s, oscillations and synchronization of the ensemble-averaged dynamics in neuronal assemblies have been found in many areas of the brain, and their roles in information processing have been discussed (For a review, see e.g. Gray (1994)). For example, when visual stimulation was given to cats, oscillations of 40 Hz appeared in the local field potential in the visual cortex. Moreover, when correlated inputs were given to the receptive fields of each assembly, synchronization among distant ($\sim$ 7mm) assemblies appeared (Gray & Singer, 1989). It has been proposed that such synchronization among neuronal assemblies might solve the binding problem (Gray, 1999). On the other hand, various oscillations are known to exist in the hippocampus, such as the sharp wave of 200 Hz (Buzsáki et al., 1992), the theta rhythm of 8 Hz (Csicsvari, Hirase, Czurko, & Buzsáki, 1998), and the gamma rhythm of 40 Hz (Bragin et al., 1995), and the correlated firing caused by such oscillations might be related to regulation of learning in the hippocampus (Buzsáki, 2006). However, the above discussions are just based on hypotheses, and possible roles and mechanisms of the oscillations and synchronization are still controversial.

Moreover, weak synchronization, where the ensemble-averaged dynamics in neuronal assemblies shows oscillations but each neuron has a low firing rate, is also known to exist in the visual cortex (Gray & Singer, 1989), in the hippocampus (Buzsáki et al., 1992; Csicsvari, Hirase, Czurko, & Buzsáki, 1998; Fisahn, Pike, Buhl, & Paulsen, 1998; Whittington et al., 2000), and in the cerebellar nucleoolivary pathway (Lang, Sugihara, & Llinás, 1996). Brunel & Hansel (2006) and Tiesinga & José (2000) called such weak synchronization as stochastic synchrony. Stochastic synchrony was found both in modeling studies based on experimental data (Traub, Miles, & Wong, 1989) and in theoretical modeling studies (Brunel, 2000; Brunel & Hakim, 1999; Brunel & Hansel, 2006; Kanamaru, 2006a; Kanamaru & Sekine, 2004), and its relationship to information processing has attracted attention. One of the mechanisms of stochastic synchrony might be oscillations with small amplitudes of the ensemble-averaged dynamics in the network. Let us consider the situation where the dynamics averaged in an assembly of neurons shows an oscillation, and this oscillation becomes a feedback input to this network. If the amplitude of this feedback input is sub-threshold for each neuron, the firing of each neuron becomes stochastic, and stochastic synchrony takes place (Kanamaru & Sekine, 2004). This mechanism is similar to that of stochastic resonance (Gammaitoni, Hänggi, Jung, & Marchesoni, 1998; Longtin, 1993).

To our knowledge, in modeling studies, stochastic synchrony has been realized only by periodic oscillations. On the other hand, in the present study, we found stochastic synchrony that was generated by chaotic oscillations. This paper is organized as follows. In section 2, a pulse coupled neural network is defined. This network is composed of excitatory neurons and inhibitory neurons, and their parameters such as synaptic time constants are set as asymmetric between excitatory and inhibitory populations in order to reflect biological conditions. Besides chemical synapses, we also introduce electrical synapses among the inhibitory neurons. To examine the dynamics of this network, the Fokker-Planck equation obtained in the limit of an infinite number of neurons is numerically analyzed, and the bifurcation of the system is investigated. By introducing electrical synapses, chaotic oscillations with small amplitudes are observed. In section 3, it is found that the oscillations with small amplitudes correspond to stochastic synchrony, namely, weak synchronization. If such oscillations are chaotic, stochastic synchrony of chaos appears. In section 4, the roles of types of connections between assemblies are examined. The final section provides discussions and conclusions.

2 A Network Composed of Excitatory Neurons and Inhibitory Neurons

In the following sections, we consider a pulse coupled neural network composed of excitatory neurons with internal states $\theta_E^{(i)}$ $(i = 1, 2, \cdots, N_E)$ and inhibitory neurons with internal states $\theta_I^{(i)}$ $(i = 1, 2, \cdots, N_I)$ (Kanamaru, 2006b) that are represented as follows:

$$\dot{\tau_E\theta_E^{(i)}} = (1 - \cos\theta_E^{(i)}) + (1 + \cos\theta_E^{(i)}) \times(r_E + \xi_E^{(i)}(t) + g_{EE}I_E(t) - g_{EI}I_I(t)), \quad (2.1)$$

$$\dot{\tau_I\theta_I^{(i)}} = (1 - \cos\theta_I^{(i)}) + (1 + \cos\theta_I^{(i)}) \times(r_I + \xi_I^{(i)}(t) + g_{IE}I_E(t) - g_{II}I_I(t) + g_{gap}I_{gap}^{(i)}(t)), \quad (2.2)$$

$$I_X(t) = \frac{1}{2N_X}\sum_{j=1}^{N_X}\sum_k \frac{1}{\kappa_X}\exp\left(-\frac{t - t_k^{(j)}}{\kappa_X}\right), \quad (2.3)$$

$$I_{gap}^{(i)}(t) = \frac{1}{N_I}\sum_{j=1}^{N_I}\sin\left(\theta_I^{(j)}(t) - \theta_I^{(i)}(t)\right), \quad (2.4)$$

$$\langle\xi_X^{(i)}(t)\xi_Y^{(j)}(t')\rangle = D\delta_{XY}\delta_{ij}\delta(t - t'), \quad (2.5)$$

where X and Y each denote the excitatory assembly E or the inhibitory assembly I, $t_k^{(j)}$ is the kth firing time of the jth neuron in assembly X, and the firing time is defined as the time at which $\theta_X^{(j)}$ exceeds π in the positive direction. In addition to the connections $I_X(t)$ by chemical synapses in which the post-synaptic potential is written by an exponential function, there are connections $I_{gap}^{(i)}(t)$ with connection strength g_{gap} by electrical synapses among the inhibitory neurons. Previous experimental studies showed that there are rich electrical synapses among inhibitory neurons in many areas of the brain such as the cortex (Galarreta & Hestrin, 1999, 2001; Gibson, Beierlein, & Connors, 1999) and the hippocampus (Fukuda & Kosaka, 2000; Katsumaru, Kosaka, Heizmann, & Hama, 1988; Strata et al., 1997; Zhang et al., 1998). The electrical synapses are realized by structures called gap junctions (Nicholls, Martin, Wallace, & Fuchs, 2001), and such connections correspond to the diffusive couplings in physical systems. It is known that they facilitate synchronous firing among neurons (Ermentrout, 2006).

Note that the model of neurons with $\dot{\theta} = (1 - \cos\theta) + (1 + \cos\theta)r$ is called the theta neuron model (Ermentrout & Kopell, 1986; Ermentrout, 1996), and this is the canonical model of class 1 neurons. Without the electrical synapses, our network is based on the canonical model of class 1 networks connected by chemical synapses with exponential functions (Izhikevich, 1999, 2000). For simplicity, the restrictions, $g_{EE} = g_{II} \equiv g_{int}$ and $g_{EI} = g_{IE} \equiv g_{ext}$, are placed, where g_{int} is the internal connection strength in an assembly and g_{ext} is the external connection strength between excitatory and inhibitory assemblies. Note that the introduction of the electrical synapses to the theta model is not straightforward because the transformation of the variable of the membrane potential to phase θ is singular when the neuron fires (Ermentrout, 2006). We use the conventional definition of the diffusive coupling for simplicity. The result similar to that obtained in this paper was also found (data not shown) using the class 1 Morris-Lecar neurons (Ermentrout, 1996; Morris & Lecar, 1981); therefore, our results might be found widely in the networks of class 1 neurons.

The membrane time constants are set as $\tau_E = 1$ and $\tau_I = 0.5$ in order to take into account the physiological fact that fast spiking cells are dominant among the inhibitory neurons in the cortex. The synaptic time constants are set as $\kappa_E = 1$ and $\kappa_I = 5$.

In the absence of inputs I_X(t) from assembly X and noise $\xi_X^{(i)}(t)$, a single neuron shows a self-oscillation when $r_X > 0$. When $r_X < 0$, this neuron becomes an excitable system with a stable equilibrium point defined by

$$\theta_0 = -\arccos\frac{1 + r_X}{1 - r_X}, \quad (2.6)$$

in which θ_0 is close to zero for $r_X \sim 0$. In the following, we use values of the parameter $r_X < 0$ and consider the dynamics of a network of excitable neurons.

As shown in Appendix A, the ensemble-averaged dynamics in this network can be analyzed using the Fokker-Planck equation (Gerstner & Kistler, 2002; Kuramoto, 1984), which is obtained in the limit of $N_E, N_I \to \infty$. When there are no correlations of firing among neurons in the network, the stable solution of the Fokker-Planck

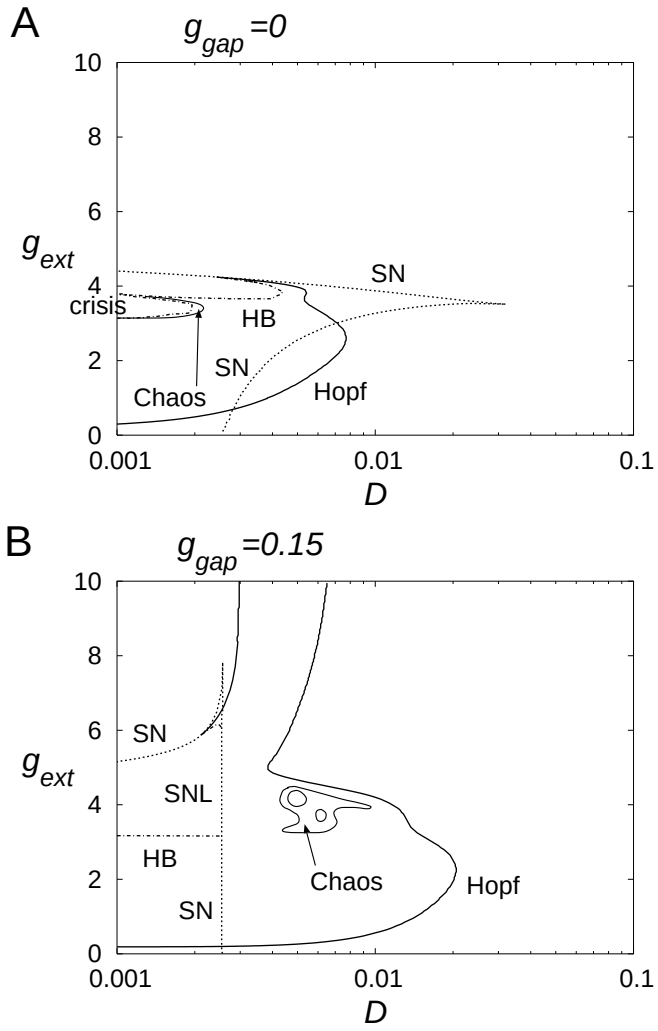

Figure 1: Bifurcation sets in the (D, g_{ext}) plane for (A) $g_{gap} = 0$ and (B) $g_{gap} = 0.15$. The excitatory and inhibitory neurons are connected by chemical synapses. Synchronous firing of neurons is generally observed when the values of D and g_{ext} are in the area enclosed by the Hopf and HB (or SNL) bifurcation lines. In (B), by introducing the electrical synapses among the inhibitory neurons, synchronous firing exists even when $g_{ext} > g_{int} = 5$. The solid, dotted, and dash-dotted lines denote the Hopf, saddle-node, and homoclinic bifurcations, respectively. The areas where a chaotic solution exists are roughly sketched. SN, the saddle-node bifurcation; SNL, the saddle-node on limit cycle bifurcation; HB, the homoclinic bifurcation.

equation is the equilibrium state. When there are some correlations of firing among neurons, the solution is time-varying, namely, the ensemble-averaged dynamics in the network can be represented by a limit cycle, a chaotic attractor, and so on. In the following, when the solution of the Fokker-Planck equation is time-varying, we consider the firing of the neurons as synchronous.

Bifurcation sets of the network obtained by numerical analyses of the Fokker-Planck equation (Kanamaru, 2006a, 2006b) based on the method given in Appendix B, are shown in Figure 1. The noise intensity D and the external connection strength g_{ext} are chosen as the bifurcation parameters. The bifurcation set for a network without electrical synapses is shown in Figure 1A. Generally, synchronous firing of neurons is observed when the values of D and g_{ext} are in the area enclosed by the Hopf and HB (or SNL) bifurcation lines. A similar analysis was presented in Kanamaru (2006b), where the membrane time constants and the synaptic time constants were set as uniform. On the other hand, in the present study, the time constants of the excitatory and inhibitory assemblies are set to be asymmetric, namely, $\tau_E = 1$, $\tau_I = 0.5$, $\kappa_E = 1$, and $\kappa_I = 5$. With this setting, it was found that the range of the parameter values where synchronous firing exists became narrower than that in the previous analysis. However, the structure of the bifurcations was almost the same with that of the previous analysis; therefore, it can be concluded that the structure of the bifurcations is robust against changes in the membrane time constants and synaptic time constants. It is also observed that chaos exists near the homoclinic bifurcation set, but the area is very narrow because chaos disappears by the crisis.

It should be also noted that synchronous firing can be observed only when $g_{ext} < g_{int} = 5$, and this fact is in agreement with a previous study (Kanamaru, 2006b). Let us consider the dynamics in a network with large g_{ext} by examining the instantaneous firing rates J_E and J_I of the excitatory and inhibitory assemblies, respectively, which can be calculated using the Fokker-Planck equation as shown in Appendix A. Generally, J_E and J_I decrease as g_{ext} increases; therefore, the equilibrium point (J_E, J_I) approaches the origin. The dependence of the equilibrium of J_E on g_{ext} is shown in Figure 2A, where J_E decreases as g_{ext} increases.

By introducing electrical synapses among the inhibitory neurons, the area where synchronous firing can be observed widened and synchronous firing was observed even for $g_{ext} > g_{int} = 5$, as shown in Figure 1B. Synchronous firing in a network with $g_{ext} > g_{int}$ was also observed when the bifurcation parameters r_E and r_I were set as asymmetric (Kanamaru, 2006a). This similarity might have arisen because electrical synapses only in the inhibitory assembly introduced asymmetry to the network. Moreover, in Figure 1B, it is also observed that the area where a chaotic solution exists widened by introducing the electrical synapses. The dependence of J_E on g_{ext} in a network with $g_{gap} = 0.15$ is shown in Figure 2B. Similarly to Figure 2A, J_E tended to decrease as g_{ext} increased. Moreover, both periodic solutions and chaotic solutions existed in networks with g_{ext} of up to 4.5, and periodic solutions appeared again in networks with $g_{ext} > 8.35$. It is also observed that in networks with relatively large g_{ext}, the periodic oscillations and the chaotic oscillations had small amplitudes near the origin. Typical chaotic oscillations in the (J_E, J_I) plane

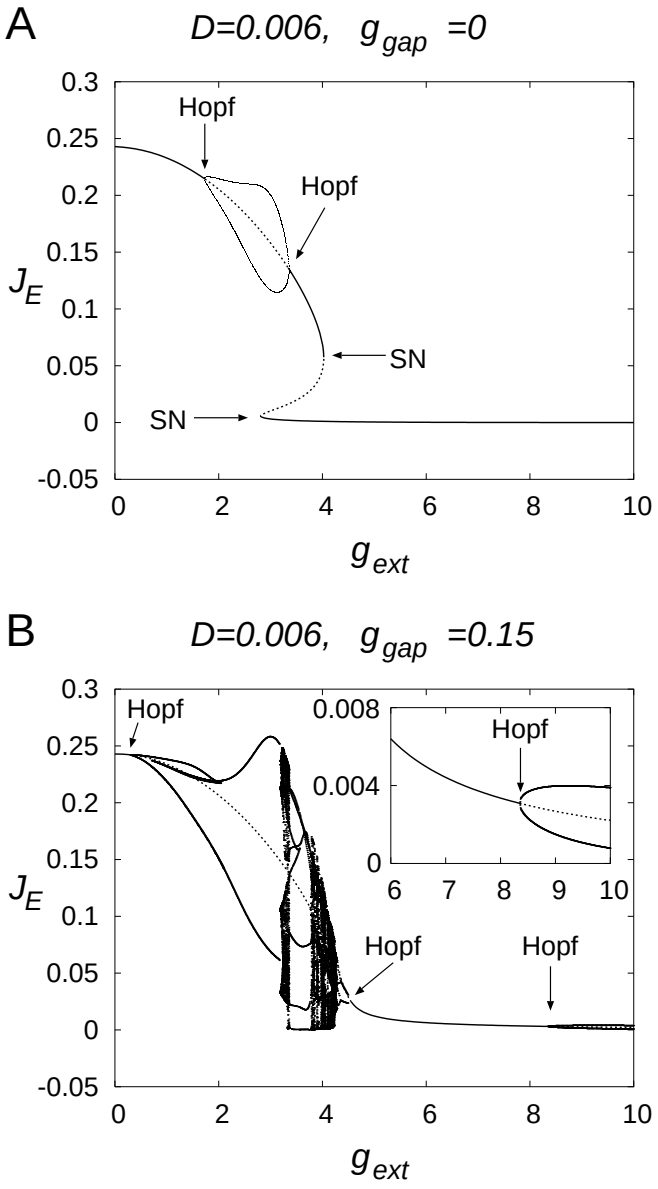

Figure 2: Dependence of the instantaneous firing rate J_E of the excitatory assembly on g_{ext}. The solid and dotted lines denote stable and unstable equilibria, respectively. When a stable limit cycles or a chaotic attractor exists in the network, their maxima and minima are also plotted. The values of the parameters are set as (A) $D = 0.006$ and $g_{gap} = 0$ and (B) $D = 0.006$ and $g_{gap} = 0.15$. The inset in (B) shows an enlargement in the range $6 \leq g_{ext} \leq 10$ where the vertical axis was expanded.

with $g_{ext} = 3.9$ or $g_{ext} = 4.4$ are shown in Figures 3A and 3B, respectively. Note that the chaotic attractor in Figure 3B is smaller than that in Figure 3A. This is because the value of g_{ext} in Figure 3B is larger than that in Figure 3A.

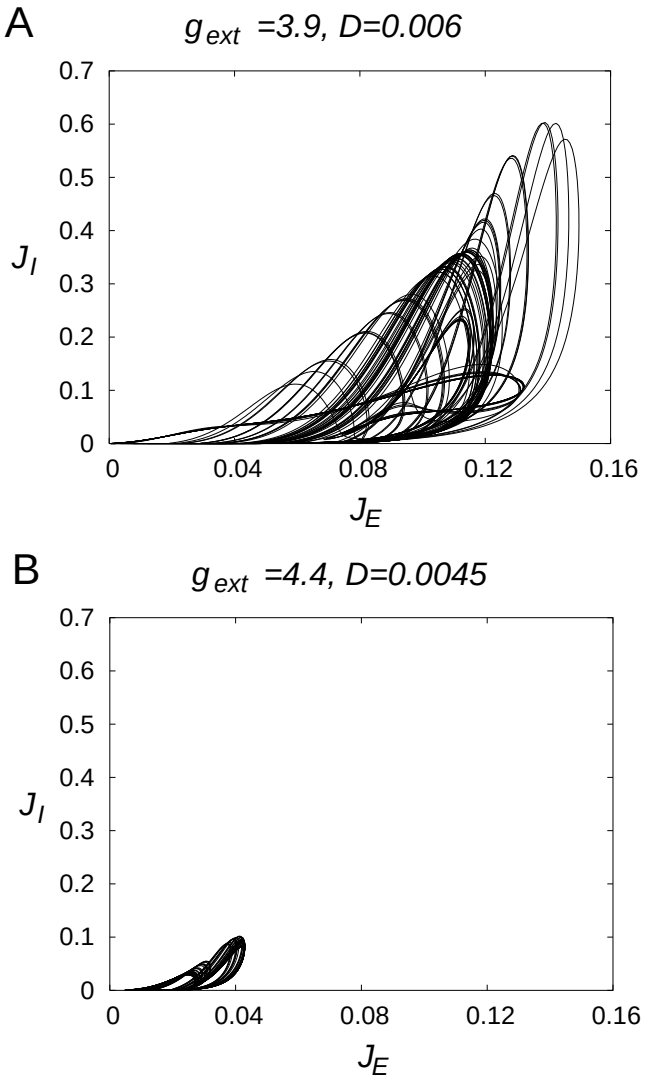

Figure 3: Chaotic attractors in the (J_E, J_I) plane for $g_{int} = 5$ and $g_{gap} = 0.15$. The values of the other parameters are set as (A) $g_{ext} = 3.9$ and $D = 0.006$ and (B) $g_{ext} = 4.4$ and $D = 0.0045$. It is observed that the attractor decreases in size as g_{ext} increases.

3 Stochastic Synchrony of Chaos

In the previous section, it was found that introduction of electrical synapses in the inhibitory assembly had the following effects on the network. First, the ranges of the parameters where periodically or chaotically synchronized firing can be observed widened. Second, the periodic or chaotic solution of the network persisted even when g_{ext} was relatively large, and such solution tended to have small amplitudes near the origin.

Note that oscillations with small amplitudes close to the origin correspond to weakly synchronized firing (Kanamaru, 2006a; Kanamaru & Sekine, 2004), where the ensemble-averaged dynamics shows synchronization in the network but each neuron has a low firing rate and the firing of each neuron seems to be stochastic. In

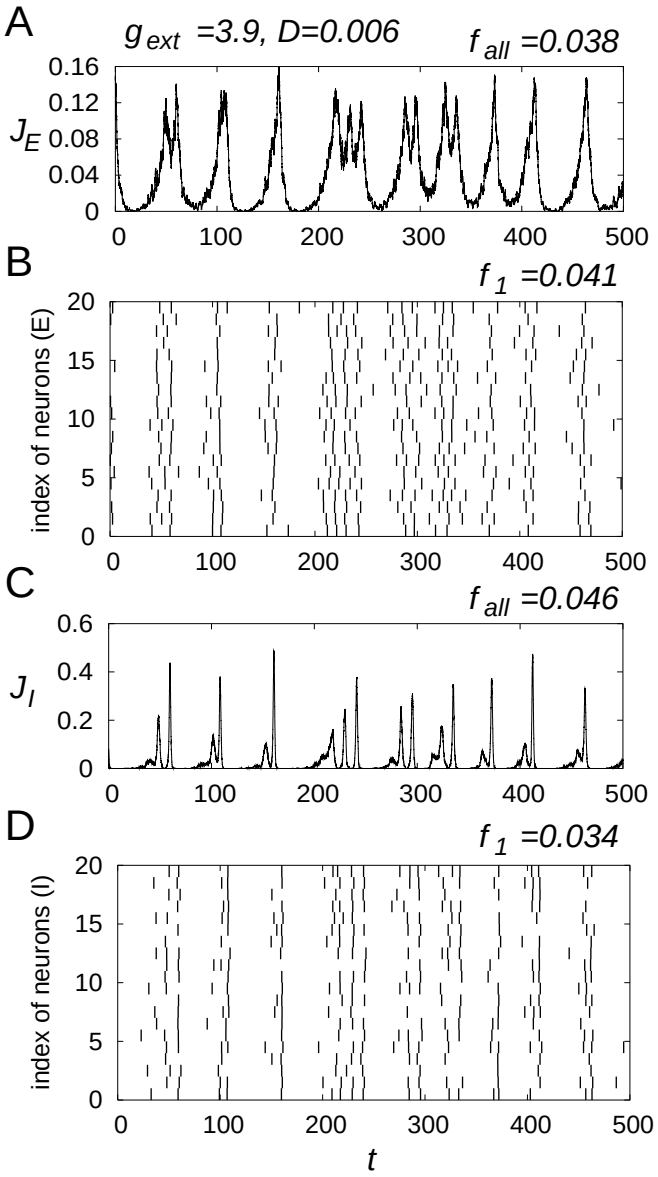

Figure 4: The firing of neurons in a finite network with $N_E = N_I = 1000$, $g_{int} = 5$, $g_{ext} = 3.9$, $g_{gap} = 0.15$, and $D = 0.006$. Note that the values of the parameters are the same with those used in Figure 3A. (A), (C) Temporal change in the instantaneous firing rate of the excitatory assembly and the inhibitory assembly, respectively. (B), (D) Raster plot of the firing times of the neurons in the excitatory assembly and in the inhibitory assembly, respectively. Each excitatory neuron fires at least once at each peak of J_E; therefore, stochastic synchrony is not observed in the excitatory assembly. On the other hand, some inhibitory neurons do not fire even when J_I takes peak values, and this phenomenon is a sign of stochastic synchrony.

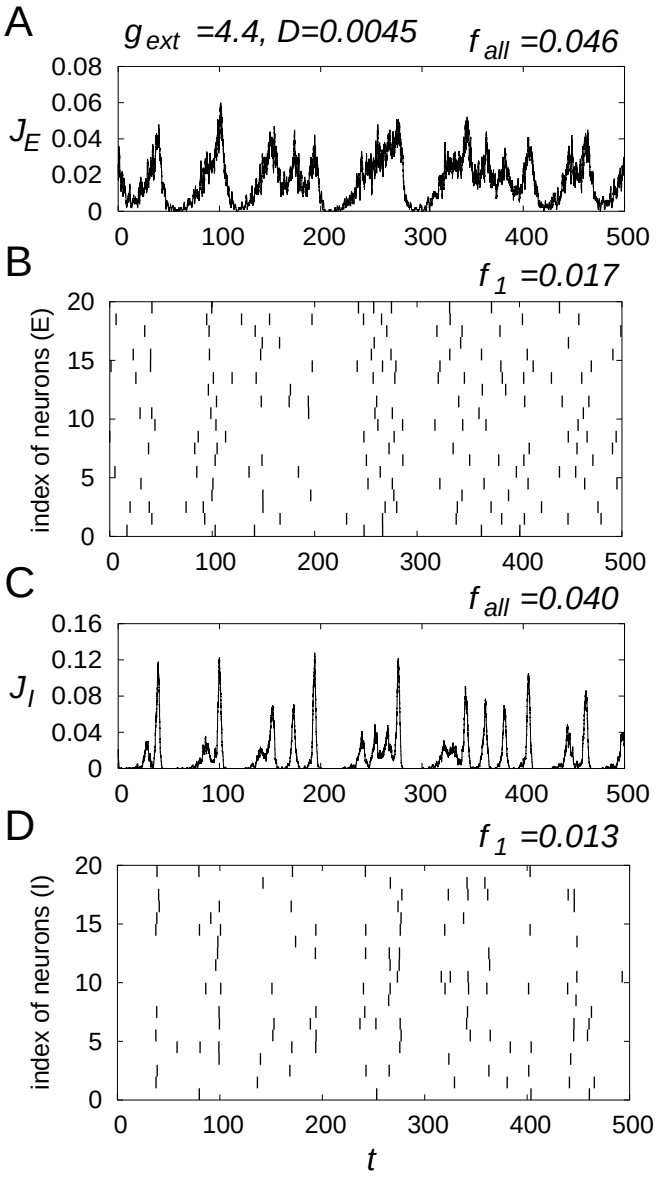

Figure 5: The firing of neurons in a finite network with $N_E = N_I = 1000$, $g_{int} = 5$, $g_{ext} = 4.4$, $g_{gap} = 0.15$, and $D = 0.0045$. Note that the values of the parameters are the same with those used in Figure 3B. (A), (C) Temporal change in the instantaneous firing rate of the excitatory assembly and the inhibitory assembly, respectively. (B), (D) Raster plot of the firing of the neurons in the excitatory assembly and in the inhibitory assembly, respectively. Stochastic synchrony of chaos is observed in both assemblies.

Brunel & Hansel (2006) and Tiesinga & José (2000), similar phenomena were called stochastic synchrony. To our knowledge, stochastic synchrony in previous studies was based on periodic oscillations, and stochastic synchrony that corresponds to chaotic oscillations, in other words, stochastic synchrony of chaos, had not been observed. Here we present the stochastic synchrony of chaos observed in our network.

First, the synchronous firing that corresponds to the chaotic attractor shown in Figure 3A, is shown in Figure 4. The trajectory shown in Figure 3A is a solution of the Fokker-Planck equation which holds in the

limit of an infinite number of neurons, and the dynamics shown in Figure 4 is the behavior of a finite network with $N_E = N_I = 1000$. The stochastic differential equations 2.1 and 2.2 are integrated numerically in Stratonovich's sense based on the method in Klauder & Petersen (1985). The instantaneous firing rate J_X in assembly X is defined as

$$J_X(t) \equiv \frac{1}{N_X d} \sum_{i=1}^{N_X} \sum_j \Theta(t - t_j^{(i)}), \qquad (3.1)$$

$$\Theta(t) = \begin{cases} 1 & \text{for } 0 \le t < d \\ 0 & \text{otherwise} \end{cases}, \qquad (3.2)$$

where $d = 1.0$. As shown in Figure 4B, each excitatory neuron fires at least once at each peak of J_E. Thus, stochastic synchrony is not observed in the excitatory neurons in the network shown in Figure 4B. To quantify this fact, we calculated the power-spectrum $P_E(f)$ of $J_E(t)$, defined by

$$P_X(f) = \frac{1}{N} \sum_{j=1}^{N} \frac{1}{T} \left| \int_{t_j}^{t_j+T} J_X(t) e^{-2\pi i f t} dt \right|^2, \qquad (3.3)$$

where $X = E$ or I, $t_1 = 0$, $t_{j+1} = t_j + T$, $T = 2048$, and $N = 21$. Note that the mean value of N samples is calculated to obtain smooth $P_X(f)$, and the frequency f has an order of $1/t$ although both f and t are dimensionless in our model. $P_E(f)$ is shown in Figure 6A, and it is observed that it has a broad spectrum because chaos and noise coexist in $J_E(t)$. Note that the peaks at small frequencies $f = 0.018$ and $f = 0.036$ denote the slow dynamics of $J_E(t)$, and the peaks at large frequencies $f = 0.075$ and $f = 0.1$ denote the fast dynamics of $J_E(t)$; therefore, the mean frequency of $J_E(t)$ would be located in the range between the frequencies which denote the slow dynamics and the fast dynamics. Based on the method shown in Appendix C, the mean frequency f_{all} of $J_E(t)$ is calculated as $f_{all} = 0.038$. On the other hand, the frequency f_1 of the firing of excitatory neurons is calculated as $f_1 = 0.041$. Because f_1 is close to f_{all}, it can be concluded that stochastic synchrony of chaos does not take place in the dynamics of the excitatory assembly shown in Figures 4A and 4B. On the other hand, some inhibitory neurons do not fire even when J_I takes peak values as shown in Figure 4D. This phenomenon is a sign of stochastic synchrony. The mean frequency f_{all} of $J_I(t)$ is calculated as $f_{all} = 0.046$, and f_1 of the firing of inhibitory neurons is calculated as $f_1 = 0.034$. Because f_1 is smaller than f_{all}, it can be concluded that stochastic synchrony of chaos takes place in the dynamics of the inhibitory assembly shown in Figures 4C and 4D.

The synchronous firing that corresponds to the chaotic attractor shown in Figure 3B, is shown in Figure 5. It is observed that both the firing of the excitatory neurons and that of the inhibitory ones are sparse and look random, and that very few neurons fire even when J_E and J_I take peak values. These firing patterns represent stochastic synchrony that corresponds to a chaotic attractor; therefore, we call these firing patterns as stochastic synchrony of chaos. The power-spectra of $J_E(t)$ and $J_I(t)$, the mean frequency f_{all} of each assembly, and the frequency f_1 of the firing of each neuron are shown in Figure 6B. In both the assemblies, it is observed that f_1 is smaller than f_{all}; therefore, it can be concluded that stochastic synchrony of chaos takes place in both the assemblies.

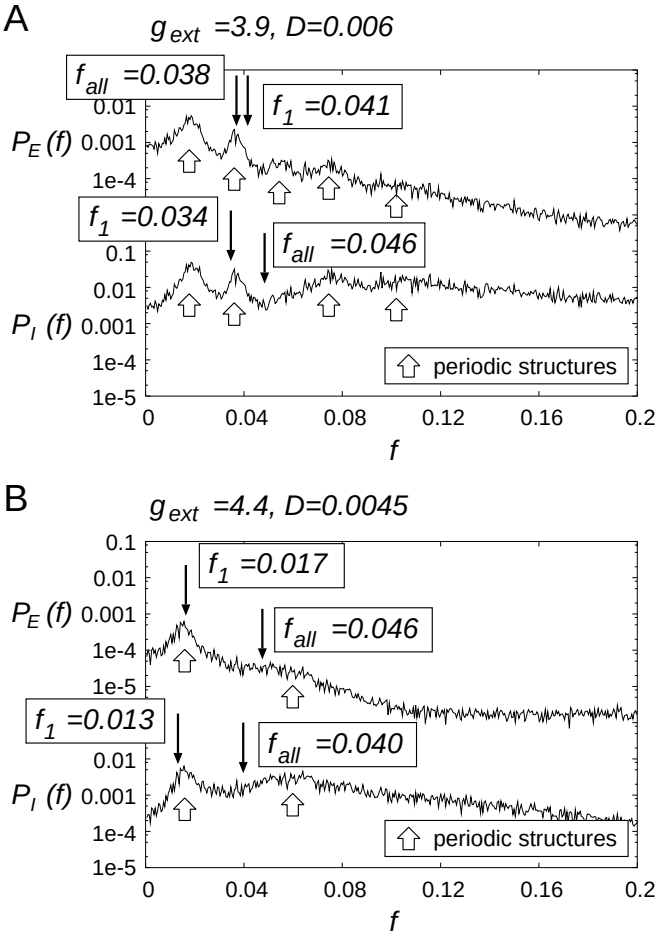

Figure 6: The power-spectra $P_E(t)$ and $P_I(f)$ of $J_E(t)$ and $J_I(t)$ in the case where (A) $g_{ext} = 3.9$ and $D = 0.006$, and (B) $g_{ext} = 4.4$ and $D = 0.0045$, which correspond to the firing patterns shown in Figure 4 and 5, respectively. Note that the frequency f has an order of $1/t$ although both f and t are dimensionless in our model. The white arrows show the positions of the periodic structures. The positions of the mean frequency f_{all} of the assembly and the frequency f_1 of the firing of each neuron are indicated by thin vertical arrows. The stochastic synchrony of chaos is observed in the inhibitory assembly in (A), and it is observed in both the assemblies in (B).

Stochastic synchrony is realized when the oscillations of the ensemble-averaged dynamics in the network have

small amplitudes as shown in Figure 3B. In such a case, the amplitude of the feedback input from the network is also small, and it causes sub-threshold oscillations for each neuron in the network and stochastic synchrony (Kanamaru & Sekine, 2004). This mechanism is similar to that of stochastic resonance (Gammaitoni, Hänggi, Jung, & Marchesoni, 1998; Longtin, 1993), which is realized when a small periodic signal and an appropriate amount of noise are injected to an excitable element. In our model, the signal and noise are defined by 2.3 and 2.5, respectively, and the periodic or chaotic signal is generated by the internal dynamics of the network.

4 Roles of Types of Connections among Neuronal Assemblies

In the previous sections, various kinds of synchronous firing including chaotic synchrony were found in the network of excitatory and inhibitory neurons by regulating the external connection strength g_{ext}. In this section, the roles of the connection strengths g_{EE}, g_{IE}, g_{EI}, and g_{II} are examined.

In the previous sections, the restrictions $g_{EE} = g_{II} = g_{int}$ and $g_{IE} = g_{EI} = g_{ext}$ were placed in order to analyze the properties of the synchronous firing in the network. In this section, we fix g_{int} and g_{ext} at values at which synchronous firing exists, and then we change the value of only one of g_{EE}, g_{IE}, g_{EI}, or g_{II} while keeping the other three values fixed. By analyzing the dependence of the average $\langle J_E \rangle$ of J_E over time and the variance $\mathrm{Var}(J_E)$ of J_E on each connection strength, the roles of each connection could be understood. Particularly, the variance $\mathrm{Var}(J_E)$ takes the value close to zero when the firing pattern of neurons is fully asynchronous, and it takes non-zero values when the firing of each neuron is synchronized. Thus, it can be used to measure the degree of synchronization.

First, let us analyze the case where there is no electrical synapse in the network ($g_{gap} = 0$). The parameters are initially fixed at $g_{EE} = g_{II} = g_{int} = 5$, $g_{IE} = g_{EI} = g_{ext} = 3$, and $D = 0.006$, where periodically synchronized firing is observed in the network. The dependence of $\langle J_E \rangle$ and $\mathrm{Var}(J_E)$ on the connection strength was analyzed by changing the value of one connection strength, and the results are shown in Figures 7A and 7B, respectively. Note that the vertical axis in Figure 7B is log-scaled, and $\mathrm{Var}(J_E)$ takes the value close to zero when there is no plot. The following properties are observed in Figure 7. First, synchronous firing disappears (i.e., $\mathrm{Var}(J_E) \sim 0$) when one connection strength is set to zero. In other words, all four types of connections are required for a genesis of synchronization. Second, strong synchronization is observed when g_{IE} and g_{EI} are smaller than g_{EE} and g_{II}. Third, adjustment of the values of g_{IE} and g_{EI} is required to observe synchronous firing because $\mathrm{Var}(J_E)$ takes non-zero values only in some ranges of g_{IE} and g_{EI} as shown in

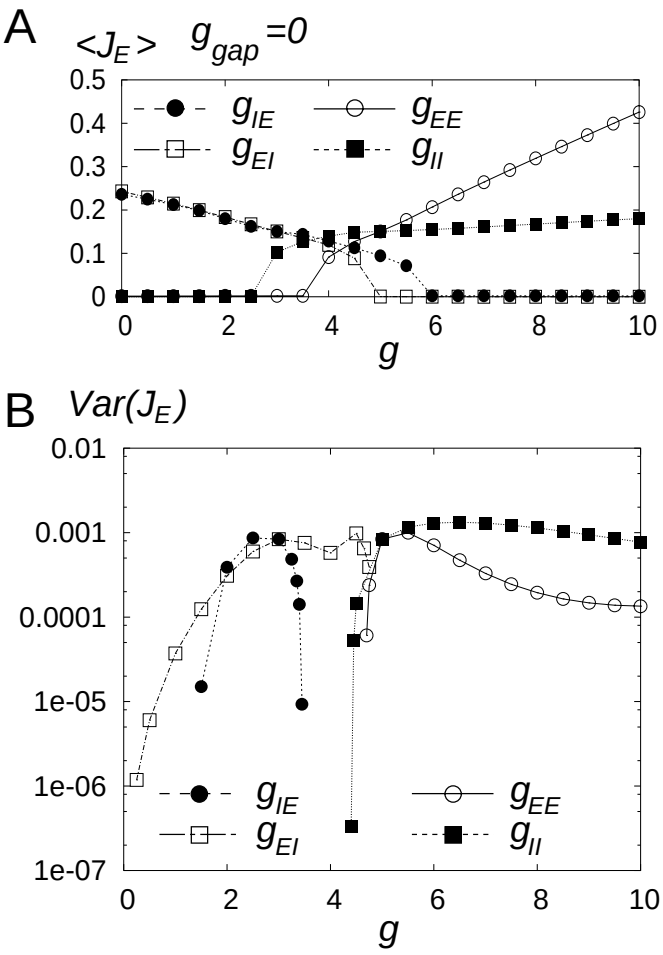

Figure 7: The dependence of (A) the average $\langle J_E \rangle$ of J_E over time and (B) the variance $\mathrm{Var}(J_E)$ of J_E on each connection strength g_{EE}, g_{II}, g_{IE}, or g_{EI}, in a network without electrical synapses. The initial values of the parameters are set as $g_{EE} = g_{II} = 5$, $g_{IE} = g_{EI} = 3$, $g_{gap} = 0$, and $D = 0.006$. The value of only one connection strength, g_{EE}, g_{II}, g_{IE}, or g_{EI}, was varied.

Figure 7B. On the other hand, as for g_{EE} and g_{II}, synchronous firing can be observed with sufficiently strong g_{EE} and g_{II}. Fourth, in networks with large g_{EE}, $\langle J_E \rangle$ increases as g_{EE} increases as shown in Figure 7A. On the other hand, in networks with large g_{II}, $\langle J_E \rangle$ remained at a nearly constant value. The above properties of synchronous firing also held for different values of g_{int}, g_{ext}, and D.

Next, we analyze the roles of the connections when there are electrical synapses in the network ($g_{gap} = 0.15$). The parameters are initially fixed at $g_{EE} = g_{II} = g_{int} = 5$, $g_{IE} = g_{EI} = g_{ext} = 4.4$, and $D = 0.0045$, where stochastic synchrony of chaos is observed in the network. Note that these values of the parameters are the same with those used in Figures 3B and 5. The dependence of $\langle J_E \rangle$ and $\mathrm{Var}(J_E)$ on each connection strength is shown in Figures 8A and 8B, respectively. There are similarities and differences compared with the

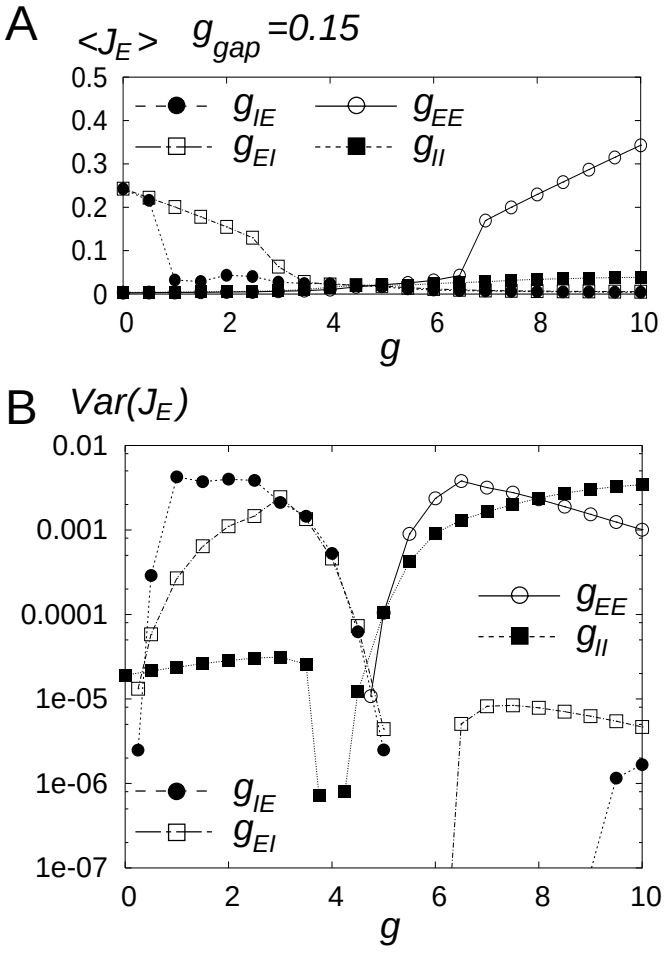

Figure 8: The dependence of (A) the average $\langle J_E \rangle$ of J_E over time and (B) the variance $\mathrm{Var}(J_E)$ of J_E on each connection strength g_{EE}, g_{II}, g_{IE}, or g_{EI}, in a network with electrical synapses. The initial values of the parameters are set as $g_{EE} = g_{II} = 5$, $g_{IE} = g_{EI} = 4.4$, $g_{gap} = 0.15$, and $D = 0.0045$. Plateau-like structures that indicate stochastic synchrony are observed in (B) for systems with small g_{II}, large g_{IE}, or large g_{EI}.

case of $g_{gap} = 0$ in Figure 7. The plateau-like structures of $\mathrm{Var}(J_E)$ observed for small g_{II}, large g_{IE}, or large g_{EI} show stochastic synchrony. This phenomenon can be understood as follows. Stochastic synchrony can be observed when g_{ext} is large as shown in Figure 1B. Therefore, it is natural that stochastic synchrony exists when g_{IE} or g_{EI} is large. Moreover, Figure 8 shows that a decrease in g_{II} has similar effects as an increase in g_{ext} in the network.

5 Discussion and Conclusions

In the present study, we analyzed the synchronous firing in a pulse coupled neural network of excitatory and inhibitory neurons that are connected by chemical synapses. Electrical synapses among the inhibitory neurons were introduced to this network. Bifurcation structure of the ensemble-averaged dynamics of neurons in the network was analyzed with the Fokker-Planck equation which is obtained in the limit of an infinite number of neurons. It was concluded that by introducing the electrical synapses to the network, the range of the parameter values where periodically or chaotically synchronized firing can be observed widened. Moreover, the periodic or chaotic solution observed in the network with electrical synapses persisted even for networks with large g_{ext}, and it was found that the solutions for networks with large g_{ext} had small amplitudes near the origin. The oscillations with small amplitudes near the origin corresponded to stochastic synchrony where the ensemble-averaged dynamics shows synchronization in the network but each neuron has a low firing rate and the firing seems to be stochastic. In the present study, we found stochastic synchrony that corresponded to a chaotic attractor, and we called this phenomenon stochastic synchrony of chaos.

The roles of the four types of connections among excitatory and inhibitory assemblies g_{EE}, g_{IE}, g_{EI}, and g_{II} were also investigated. It was found that in a network without electrical synapses, all four types of connections were required for a genesis of synchronous firing. This result seems to contradict the previous finding that the pulse coupled self-oscillating neurons can perfectly or partially synchronize with each other without inhibitory neurons (Hansel, Mato, & Meunier, 1995; Kuramoto, 1991; Mirollo & Strogatz, 1990; Tsodyks, Mitkov, & Sompolinsky, 1993; van Vreeswijk, 1996) or without excitatory neurons (Golomb & Rinzel, 1993; Kopell, 2000; van Vreeswijk, Abbott & Ermentrout, 1994). This discrepancy is caused by the fact that our network is composed of excitable, not self-oscillating neurons. In addition, it was found that adjustment of g_{EI} and g_{IE} was required. As to networks with electrical synapses, stochastic synchrony was observed in networks with small g_{II}, large g_{IE}, or large g_{EI}.

Although stochastic synchrony is often observed in sparsely connected networks (Brunel, 2000; Brunel & Hakim, 1999; Traub, Miles, & Wong, 1989), all neurons in our network were connected with each other and the connections were uniform. Thus, it can be concluded that randomness of connections is not required for a genesis of stochastic synchrony. Moreover, there are cases in which stochastic synchrony is observed both in the excitatory assembly and in the inhibitory assembly (Figures 5B and 5D). This was observed because the peak values of both J_E and J_I were small. It is inferred that there would be cases where stochastic synchrony is observed either in the excitatory assembly or in the inhibitory assembly according to the shape of the attractor.

When stochastic synchrony exists in a network, the contribution of a single neuron in the network to the synchronization is small. Therefore, this neuron might also contribute to form other synchronous networks simultaneously. If such dynamics is realized, they can be

interpreted as the stochastic realization of the dynamical cell assemblies (Fujii et al., 1996; Hebb, 1949). Investigation of such dynamics is an important future problem.

Acknowledgement

This study was partially supported by a Grant-in-Aid for Encouragement of Young Scientists (B) (No. 17700226) and a Grant-in-Aid for Scientific Research on Priority Areas (No. 17022012) from The Ministry of Education, Culture, Sports, Science and Technology of Japan.

A The Fokker-Planck Equation for the System

To analyze the dynamics of the network, we use the Fokker-Planck equations (Gerstner & Kistler, 2002; Kuramoto, 1984) which are represented as

$$\begin{aligned}
\frac{\partial n_E}{\partial t} &= -\frac{\partial}{\partial \theta_E}(A_E n_E) \\
&\quad + \frac{D}{2}\frac{\partial}{\partial \theta_E}\left\{ B_E \frac{\partial}{\partial \theta_E}(B_E n_E) \right\}, \qquad \text{(A.1)} \\
\frac{\partial n_I}{\partial t} &= -\frac{\partial}{\partial \theta_I}(A_I n_I) \\
&\quad + \frac{D}{2}\frac{\partial}{\partial \theta_I}\left\{ B_I \frac{\partial}{\partial \theta_I}(B_I n_I) \right\}, \qquad \text{(A.2)} \\
A_E(\theta_E, t) &= \frac{1}{\tau_E}(1-\cos\theta_E) + \frac{1}{\tau_E}(1+\cos\theta_E) \\
&\quad \times (r_E + g_{EE} I_E(t) - g_{EI} I_I(t)), \qquad \text{(A.3)} \\
A_I(\theta_I, t) &= \frac{1}{\tau_I}(1-\cos\theta_I) + \frac{1}{\tau_I}(1+\cos\theta_I) \\
&\quad \times (r_I + g_{IE} I_E(t) - g_{II} I_I(t) + g_{gap} I_{gap}(\theta_I, t)), \qquad \text{(A.4)} \\
B_E(\theta_E, t) &= \frac{1}{\tau_E}(1+\cos\theta_E), \qquad \text{(A.5)} \\
B_I(\theta_I, t) &= \frac{1}{\tau_I}(1+\cos\theta_I), \qquad \text{(A.6)} \\
I_{gap}(\theta_I, t) &= \langle \sin\theta_I \rangle \cos\theta_I - \langle \cos\theta_I \rangle \sin\theta_I, \qquad \text{(A.7)} \\
\langle f(\theta_I) \rangle &= \int_0^{2\pi} f(\theta_I)\, n_I(\theta_I, t)\, d\theta_I, \qquad \text{(A.8)}
\end{aligned}$$

for the normalized number densities of excitatory and inhibitory neurons, in which

$$\begin{aligned}
n_E(\theta_E, t) &\equiv \frac{1}{N_E}\sum \delta(\theta_E^{(i)} - \theta_E), \qquad \text{(A.9)} \\
n_I(\theta_I, t) &\equiv \frac{1}{N_I}\sum \delta(\theta_I^{(i)} - \theta_I), \qquad \text{(A.10)}
\end{aligned}$$

in the limit of $N_E, N_I \to \infty$. The probability flux for each assembly is defined as

$$\begin{aligned}
J_E(\theta_E, t) &= A_E n_E - \frac{D}{2} B_E \frac{\partial}{\partial \theta_E}(B_E n_E), \qquad \text{(A.11)} \\
J_I(\theta_I, t) &= A_I n_I - \frac{D}{2} B_I \frac{\partial}{\partial \theta_I}(B_I n_I), \qquad \text{(A.12)}
\end{aligned}$$

respectively. In the limit of $N_X \to \infty$, $I_X(t)$ in equation 2.3 follows the following differential equation,

$$\dot{I_X}(t) = -\frac{1}{\kappa_X}\left(I_X(t) - \frac{1}{2} J_X(t) \right), \qquad \text{(A.13)}$$

where $J_X(t) \equiv J_X(\pi, t)$ is the probability flux at $\theta_X = \pi$.

By integrating the Fokker-Planck equations A.1 and A.2 and the differential equation A.13 simultaneously, the dynamics of the network that is governed by equations 2.1 and 2.2 can be analyzed.

B Numerical Integration of the Fokker-Planck Equations

In this section, we provide a method on the numerical integration of the Fokker-Planck equations A.1 and A.2. Because the normalized number densities given by equations A.9 and A.10 are 2π-periodic functions of θ_E and θ_I, respectively, they can be expanded as

$$\begin{aligned}
n_E(\theta_E, t) &= \frac{1}{2\pi} + \sum_{k=1}^{\infty} (a_k^E(t)\cos(k\theta_E) + b_k^E(t)\sin(k\theta_E)), \qquad \text{(B.1)} \\
n_I(\theta_I, t) &= \frac{1}{2\pi} + \sum_{k=1}^{\infty} (a_k^I(t)\cos(k\theta_I) + b_k^I(t)\sin(k\theta_I)), \qquad \text{(B.2)}
\end{aligned}$$

and, by substituting them, equations A.1 and A.2 are transformed into a set of ordinary differential equations of a_k^X and b_k^X as follows:

$$\begin{aligned}
\frac{da_k^{(X)}}{dt} &= -(r_X + \tilde{I}_X + 1)\frac{k}{\tau_X} b_k^{(X)} \\
&\quad -(r_X + \tilde{I}_X - 1)\frac{k}{2\tau_X}(b_{k-1}^{(X)} + b_{k+1}^{(X)}) \\
&\quad -\frac{Dk}{8\tau_X^2} f(a_k^{(X)}) \\
&\quad +\frac{\pi g_{gap} k}{4\tau_X}(-b_1 g_1(b_k^{(X)}) + a_1 g_2(a_k^{(X)}))\delta_{XI}, \qquad \text{(B.3)} \\
\frac{db_k^{(X)}}{dt} &= (r_X + \tilde{I}_X + 1)\frac{k}{\tau_X} a_k^{(X)} \\
&\quad +(r_X + \tilde{I}_X - 1)\frac{k}{2\tau_X}(a_{k-1}^{(X)} + a_{k+1}^{(X)}) \\
&\quad -\frac{Dk}{8\tau_X^2} f(b_k^{(X)}) \\
&\quad +\frac{\pi g_{gap} k}{4\tau_X}(b_1 g_1(a_k^{(X)}) + a_1 g_2(b_k^{(X)}))\delta_{XI}, \qquad \text{(B.4)} \\
f(x_k) &= (k-1)x_{k-2} + 2(2k-1)x_{k-1} + 6kx_k \\
&\quad +2(2k+1)x_{k+1} + (k+1)x_{k+2}, \qquad \text{(B.5)} \\
g_1(x_k) &= x_{k-2} + 2x_{k-1} + 2x_k + 2x_{k+1} + x_{k+2}, \qquad \text{(B.6)}
\end{aligned}$$

$$g_2(x_k) = x_{k-2} + 2x_{k-1} - 2x_{k+1} - x_{k+2}, \quad \text{(B.7)}$$

$$\tilde{I}_X \equiv g_{XE} I_E - g_{XI} I_I, \quad \text{(B.8)}$$

$$a_0^{(X)} \equiv \frac{1}{\pi}, \quad \text{(B.9)}$$

$$b_0^{(X)} \equiv 0, \quad \text{(B.10)}$$

$$a_{-n}^{(X)} \equiv a_n^{(X)}, \quad \text{(B.11)}$$

$$b_{-n}^{(X)} \equiv -b_n^{(X)}, \quad \text{(B.12)}$$

where $X = E$ or I. Using a vector $\boldsymbol{x} = (I_E, I_I, a_1^E, b_1^E, a_1^I, b_1^I, a_2^E, b_2^E, a_2^I, b_2^I, \cdots)^t$, the ordinary differential equations $\dot{\boldsymbol{x}} = \boldsymbol{f}(\boldsymbol{x})$ are defined by A.13, B.3, and B.4. By integrating this ordinary differential equations numerically, the time series of the probability fluxes J_E and J_I are obtained. For numerical calculations, each Fourier series is truncated at the first 40 or 60 terms.

The bifurcation sets of the Hopf bifurcation and the saddle-node bifurcation in Figure 1 were obtained as follows. A stationary solution $\boldsymbol{x}_s$ was numerically obtained by the Newton method (Press, Flannery, Teukolsky, & Vetterling, 1988), and the eigenvalues of the Jacobian matrix $D\boldsymbol{f}(\boldsymbol{x}_s)$ that had been numerically obtained by using the QR algorithm (Press, Flannery, Teukolsky, & Vetterling, 1988), were examined to find the bifurcation sets. On the other hand, the bifurcation sets of the homoclinic bifurcation were obtained by observing the long-time behaviors of the solutions of $\dot{\boldsymbol{x}} = \boldsymbol{f}(\boldsymbol{x})$.

C Derivation of the Mean Frequency of the Assembly

In this section, we provide a method on the numerical calculation of the mean frequency f_{all} of the assembly in the network with a finite number of neurons. As shown in Figures 4A, 4C, 5A, and 5C, $J_X(t)$ ($X = E$ or I) of the finite network is noisy. To eliminate noise, we use the the low-pass filter written by

$$\dot{x}_{out} = -\frac{1}{\tau} x_{out} + \frac{1}{\tau} x_{in}, \quad \text{(C.1)}$$

where x_{in} and x_{out} are the input and the output of this filter, respectively, and its cutoff frequency is defined by

$$f_c = \frac{1}{2\pi\tau}. \quad \text{(C.2)}$$

The cutoff frequency f_c is set at the maximal frequency where the peak of the power-spectrum is observed, namely, $f_c = 0.1$ for $g_{ext} = 3.9$ and $D = 0.006$ in Figure 6A, and $f_c = 0.06$ for $g_{ext} = 4.4$ and $D = 0.0045$ in Figure 6B. After applying this low-pass filter to $J_X(t)$ twice, we count the number of peaks of $J_X(t)$. $J_X(t^*)$ at $t = t^*$ is considered as a peak when two conditions $J_X(t^*) > J_X(t^* \pm \Delta t)$ and $J_X(t^*) > \langle J_X(t) \rangle$ are satisfied, where Δt is the time step of data, and $\langle J_X(t) \rangle$ is the time-average of $J_X(t)$. The second condition was required to avoid spurious peaks caused by noise. After counting the peaks, we define the mean frequency f_{all} of the assembly as the number of peaks of $J_X(t)$ per unit time.

References

Bragin, A., Jandó, G., Nádasdy, Z., Hetke, J., Wise, K., & Buzsáki, G. (1995). Gamma (40-100 Hz) oscillation in the hippocampus of the behaving rat. *The Journal of Neuroscience*, 15, 47–60.

Brunel, N. (2000). Dynamics of sparsely connected networks of excitatory and inhibitory spiking neurons. *Journal of Computational Neuroscience*, 8, 183–208.

Brunel, N. & Hakim, V. (1999). Fast global oscillations in networks of integrate-and-fire neurons with low firing rates. *Neural Comput.*, 11, 1621–1671.

Brunel, N. & Hansel, D. (2006). How noise affects the synchronization properties of recurrent networks of inhibitory neurons. *Neural Comput.*, 18, 1066–1110.

Buzsáki, G. (2006). *Rhythms of the brain*, (Oxford University Press, New York).

Buzsáki, G., Horváth, Z., Urioste, R., Hetke, J., & Wise, K. (1992). High-frequency network oscillation in the hippocampus. *Science*, 256, 1025–1027.

Csicsvari, J., Hirase, H., Czurko, A., & Buzsáki, G. (1998). Reliability and state dependence of pyramidal cell-interneuron synapses in the hippocampus: an ensemble approach in the behaving rat. *Neuron*, 21, 179–189.

Ermentrout, B. (1996). Type I membranes, phase resetting curves, and synchrony. *Neural Comput.*, 8, 979–1001.

Ermentrout, B. (2006). Gap junctions destroy persistent states in excitatory networks. *Phys. Rev. E*, 74, 031918.

Ermentrout, G. B., & Kopell, N. (1986). Parabolic bursting in an excitable system coupled with a slow oscillation. *SIAM J. of Appl. Math.*, 46, 233–253.

Fisahn, A., Pike, F. G., Buhl, E. H., & Paulsen, O. (1998). Cholinergic induction of network oscillations at 40 Hz in the hippocampus in vitro. *Nature*, 394, 186–189.

Fujii, H., Ito, H., Aihara, K., Ichinose, N., & Tsukada, M. (1996). Dynamical cell assembly hypothesis –

Theoretical possibility of spatio-temporal coding in the cortex. *Neural Networks*, 9, 1303–1350.

Fukuda, T., & Kosaka, T. (2000). Gap junctions linking the dendritic network of GABAergic interneurons in the hippocampus. *The Journal of Neuroscience*, 20, 1519–1528.

Galarreta, M. & Hestrin, S. (1999). A network of fast-spiking cells in the neocortex connected by electrical synapse. *Nature*, 402, 72–75.

Galarreta, M. & Hestrin, S. (2001). Electrical synapses between GABA-releasing interneurons. *Nature Reviews Neuroscience*, 2, 425–433.

Gammaitoni, L., Hänggi, P., Jung, P., & Marchesoni, F. (1998). Stochastic resonance. *Reviews of Modern Physics*, 70, 223–287.

Gerstner, W. & Kistler, W. (2002). *Spiking Neuron Models* (Cambridge Univ. Press, Cambridge).

Gibson, J. R., Beierlein, M., & Connors, B. W. (1999). Two networks of electrically coupled inhibitory neurons in neocortex. *Nature*, 402, 75–79.

Golomb, D. & Rinzel, J. (1993). Dynamics of globally coupled inhibitory neurons with heterogeneity. *Physical Review E*, 48, 4810–4814.

Gray, C. M. (1994). Synchronous oscillations in neuronal systems: mechanisms and functions. *J. Comput. Neurosci.*, 1, 11–38.

Gray, C. M. (1999). The temporal correlation hypothesis of visual feature integration: still alive and well. *Neuron*, 24, 31–47.

Gray, C. M. & Singer, W. (1989). Stimulus-specific neuronal oscillations in orientation columns of cat visual cortex. *Proc. Natl. Acad. Sci. USA*, 86, 1698–1702.

Hansel, D., Mato, G., & Meunier, C. (1995) Synchrony in excitatory neural networks. *Neural Comput.*, 7, 307–337.

Hebb, D. O. (1949). *The Organization of Behavior – a neuropsychological theory* (John Wiley, New York).

Izhikevich, E. M. (1999). Class 1 neural excitability, conventional synapses, weakly connected networks, and mathematical foundations of pulse-coupled models. *IEEE Trans. Neural Networks*, 10, 499–507.

Izhikevich, E. M. (2000). Neural excitability, spiking and bursting. *Int. J. Bifurcation and Chaos*, 10, 1171–1266.

Kanamaru, T. (2006a). Analysis of synchronization between two modules of pulse neural networks with excitatory and inhibitory connections. *Neural Comput.*, 18, 1111–1131.

Kanamaru, T. (2006b). Blowout bifurcation and on-off intermittency in pulse neural networks with multiple modules. *Int. J. Bifurcation and Chaos*, 16, 3309–3321.

Kanamaru, T. & Sekine, M. (2004). An analysis of globally connected active rotators with excitatory and inhibitory connections having different time constants using the nonlinear Fokker-Planck equations. *IEEE Transactions on Neural Networks*, 15, 1009–1017.

Katsumaru, H., Kosaka, T., Heizmann, C. W., & Hama, K. (1988). Gap junctions on GABAergic neurons containing the calcium-binding protein parvalbumin in the rat hippocampus (CA1 region). *Experimental Brain Research*, 72, 363–370.

Klauder, J. R. & Petersen, W. P. (1985). Numerical integration of multiplicative-noise stochastic differential equations. *SIAM J. Numer. Aanal.*, 22, 1153–1166.

Kopell, N. (2000). We got rhythm: dynamical systems of the nervous system. *Notices of the AMS*, 47, 6–16.

Kuramoto, Y. (1984). *Chemical oscillations, waves, and turbulence* (Springer, Berlin).

Kuramoto, Y. (1991). Collective synchronization of pulse-coupled oscillators and excitable units. *Physica D*, 50, 15–30.

Lang, E. J., Sugihara, I., & Llinás, R. (1996). GABAergic modulation of complex spike activity by the cerebellar nucleoolivary pathway in rat. *Journal of Neurophysiology*, 76, 255–275.

Longtin, A. (1993). Stochastic resonance in neuron models. *Journal of Statistical Physics*, 70, 309–327.

Mirollo, R. E. & Strogatz, S. H. (1990). Synchronization of pulse-coupled biological oscillators. *SIAM Journal of Applied Mathematics*, 50, 1645–1662.

Morris, C. & Lecar, H. (1981). Voltage oscillations in the barnacle giant muscle fiber. *Biophys. J.*, 35,

193–213.

Nicholls, J. G., Martin, A. R., Wallace, B. G., & Fuchs, P. A. (2001). *From Neuron to Brain*. Sinauer Associates Inc. Publishers, Massachusetts.

Press, W. H., Flannery, B. P., Teukolsky, S. A., & Vetterling, W. T. (1988). *Numerical Recipes in C*, Cambridge Univ. Press, New York.

Strata, F., Atzori, M., Molnar, M., Ugolini, G., Tempia, F., & Cherubini, E. (1997). A pacemaker current in dye-coupled hilar interneurons contributes to the generation of giant GABAergic potentials in developing hippocampus. *The Journal of Neuroscience*, 17, 1435–1446.

Tiesinga, P. H. E., & José, J. V., (2000). Robust gamma oscillations in networks of inhibitory hippocampal interneurons. *Network*, 11, 1-23.

Traub, R. D., Miles, R., & Wong, K. S., (1989). Model of the origin of rhythmic population oscillations in the hippocampal slice. *Science*, 243, 1319–1325.

Tsodyks, M., Mitkov, I., & Sompolinsky, H. (1993). Pattern of synchrony in inhomogeneous networks of oscillators with pulse interactions. *Physical Review Letters*, 71, 1280–1283.

van Vreeswijk, C. (1996) Partial synchronization in populations of pulse-coupled oscillators. *Physical Review E*, 54, 5522–5537.

van Vreeswijk, C., Abbott, L. F., & Ermentrout, G. B. (1994). When inhibition not excitation synchronizes neural firing. *Journal of Computational Neuroscience*, 1, 313–321.

Whittington, M. A., Traub, R. D., Kopell, N., Ermentrout, B., & Buhl, E. H., (2000). Inhibition-based rhythms: experimental and mathematical observations on network dynamics. *International Journal of Psychophysiology*, 38, 315–336.

Zhang, Y., Velazquez, J. L. P., Tian, G. F., Wu, C.-P., Skinner, F. K., Carlen, P. L., & Zhang, L. (1998). Slow oscillations ($\leq$ 1 Hz) mediated by GABAergic interneuronal networks in rat hippocampus. *The Journal of Neuroscience*, 15, 9256–9268.